

# Sustained Release of Magnesium Ions Mediated by a Dynamic Mechanical Hydrogel to Enhance BMSC Proliferation and Differentiation

Jiayu Liu, Hongli Zeng, Peng Xiao, Anqun Yang, Xingxian Situ, Yao Wang, Xiang Zhang, Wenqiang Li,\* Weiyi Pan,\* and Yulong Wang\*



Cite This: *ACS Omega* 2020, 5, 24477–24486

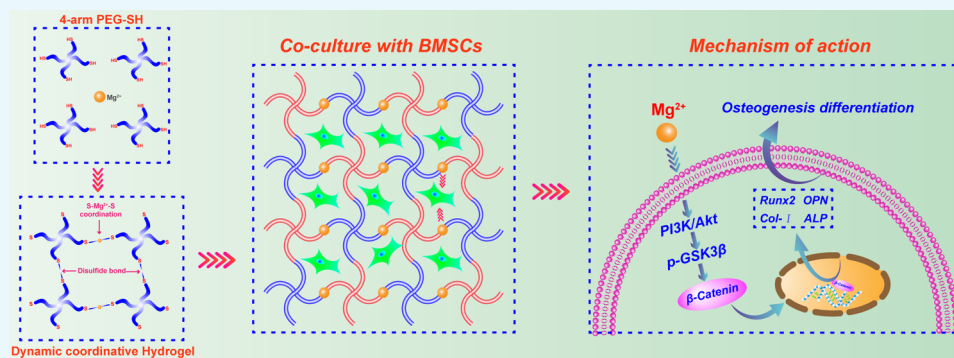


Read Online

ACCESS |

Metrics & More

Article Recommendations



**ABSTRACT:** Hydrogel scaffolds are promising and widely applicable platforms for various therapeutic agents to facilitate bone tissue regeneration due to their biocompatibility and low immunogenicity. Nevertheless, the improvement of local administration efficiency and on-demand release of drugs from a hydrogel system is still an obstacle. In this work, we reported that a novel injectable hydrogel system was fabricated based on coordination of multiarm thiolated polyethylene glycol (PEG-SH) and magnesium ions for bone marrow-derived mesenchymal stem cell (BMSC) proliferation and differentiation. The dynamic nature coordination bond of Mg–S and the dynamic disulfide bond of S–S provide hydrogels with good mechanical performance and typical rheological behavior and thus endow the hydrogels with a satisfactory swelling rate and degradation property.  $Mg^{2+}$  was incorporated in the system not only to act as an effective cross-linker to enhance the hydrogel network structure but also to mediate the sustained release of  $Mg^{2+}$ . Due to the controlled release of  $Mg^{2+}$ , the PEG-SH/ $Mg^{2+}$  hydrogel can effectively improve BMSC proliferation and osteoblastic activity via the PI3K/Akt/GSK3 $\beta$ / $\beta$ -catenin signal pathway in vitro. These findings indicated that the novel hydrogel controlled release of a  $Mg^{2+}$  ion is viewed as a promising and flexible platform for bone regeneration clinically.

## 1. INTRODUCTION

Nowadays, due to injuries or diseases, large numbers of patients with bone defects continue to emerge. Realizing efficient bone healing has increasingly become a focus of widespread concern. Therefore, it is necessary to promote bone defect regeneration by constructing effective strategies. Inspired by a native bone extracellular matrix (ECM), developing functional scaffolds with a biomimetic component and a biomimetic structure to reconstruct the bone tissue injuries has drawn much attention.<sup>1–3</sup> In recent years, a hydrogel was used as a promising substitute for bone scaffold material because of its good cell compatibility, adjustable biodegradability, capability to offer a three-dimensional (3D) porous network, and therapeutical properties, providing an ideal platform for cell proliferation and migration. Thus, hydrogel scaffolds have become a promising strategy in bone

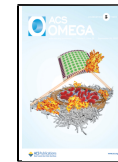
regenerative medicine.<sup>4–7</sup> However, a large number of polymer hydrogels usually has weak biomechanics and poor differentiation ability of osteoblasts, which is adverse to osteoconductivity.<sup>8–10</sup>

A magnesium ion is an important cation in the human body, participating in various metabolisms in the body, regulating bone metabolism activities, which is related to the reconstruction and stability of bone tissue.<sup>11–16</sup> For example, Zhang et al. proposed incorporated particles composite

Received: June 18, 2020

Accepted: September 4, 2020

Published: September 16, 2020



**Scheme 1.** Schematic Illustration of the PEG-SH/Mg<sup>2+</sup> Hydrogel Preparation Process and the Mechanism Action of Mg<sup>2+</sup> for Targeting BMSC Differentiation via the PI3K/Akt/p-GSK3β/β-Catenin Pathway

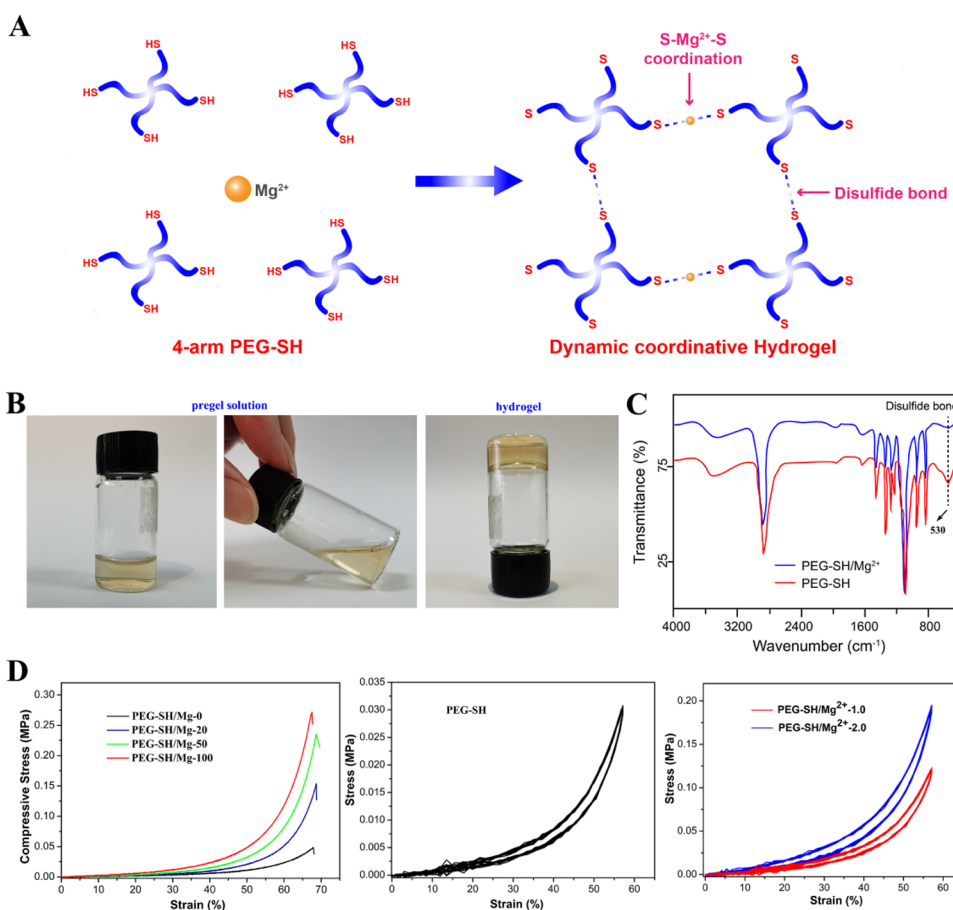
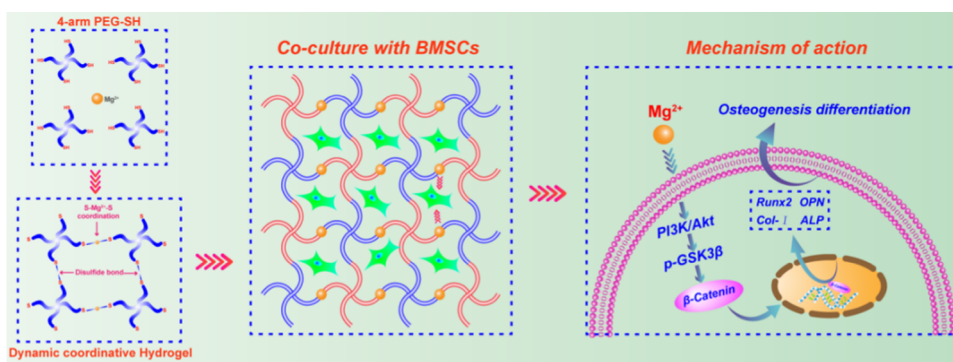


**Figure 1.** (A) Schematic illustration of the Mg<sup>2+</sup>-thiol coordinative hydrogel fabricated by blending 4-arm-PEG-SH with MgCl<sub>2</sub>, (B) photographs of the gelation process of the hydrogel, (C) FTIR spectra of PEG-SH and PEG-SH/Mg<sup>2+</sup> samples, (D) compression stress-strain curves of PEG-SH, PEG-SH/Mg<sup>2+</sup>-1.0, and PEG-SH/Mg<sup>2+</sup>-2.0 hydrogels, and the corresponding cyclic compressive stress-strain curves at 60% strain.

hydrogels based on self-assembly driven by bisphosphonate-Mg<sup>2+</sup> coordination to stimulate cell spreading and osteogenesis.<sup>17</sup> Another injectable composite hydrogel scaffold can maintain the controlled release of Mg<sup>2+</sup> ions and promote bone formation.<sup>18</sup> Although adding Mg<sup>2+</sup> to a system has been demonstrated to accelerate new bone generation, the exact mechanisms underlying the stimulatory effect of magnesium on osteogenesis remains to be elusive.<sup>19,20</sup> The previous studies demonstrated that the TRPM7/PI3K signaling pathway,<sup>21</sup> Notch signaling pathway,<sup>22</sup> and Wnt/β-catenin signaling pathway<sup>23</sup> are clearly caused by a magnesium ion.<sup>24</sup> However, the influence of the Wnt/β-catenin signaling pathway on

osteogenic differentiation has almost not been reported. In addition, there are some studies that have indicated that Mg<sup>2+</sup> ions possess the capacity to affect the osteoblasts of mesenchymal stem cells via the PI3K/Akt pathway-related genes.<sup>25,26</sup> It has been discovered that different amounts of Mg<sup>2+</sup> ions affect the PI3K/Akt signal in osteoblasts.<sup>27,28</sup> Mg<sup>2+</sup> ions can result in a series of changes in bone tissue-related signaling molecules by activating PI3K/Akt signaling pathways, such as promoting osteogenic differentiation markers such as alkaline phosphatase and bone morphogenetic protein expression. However, the function of PI3K/Akt signaling pathways in the promotion of bone tissue repair has been

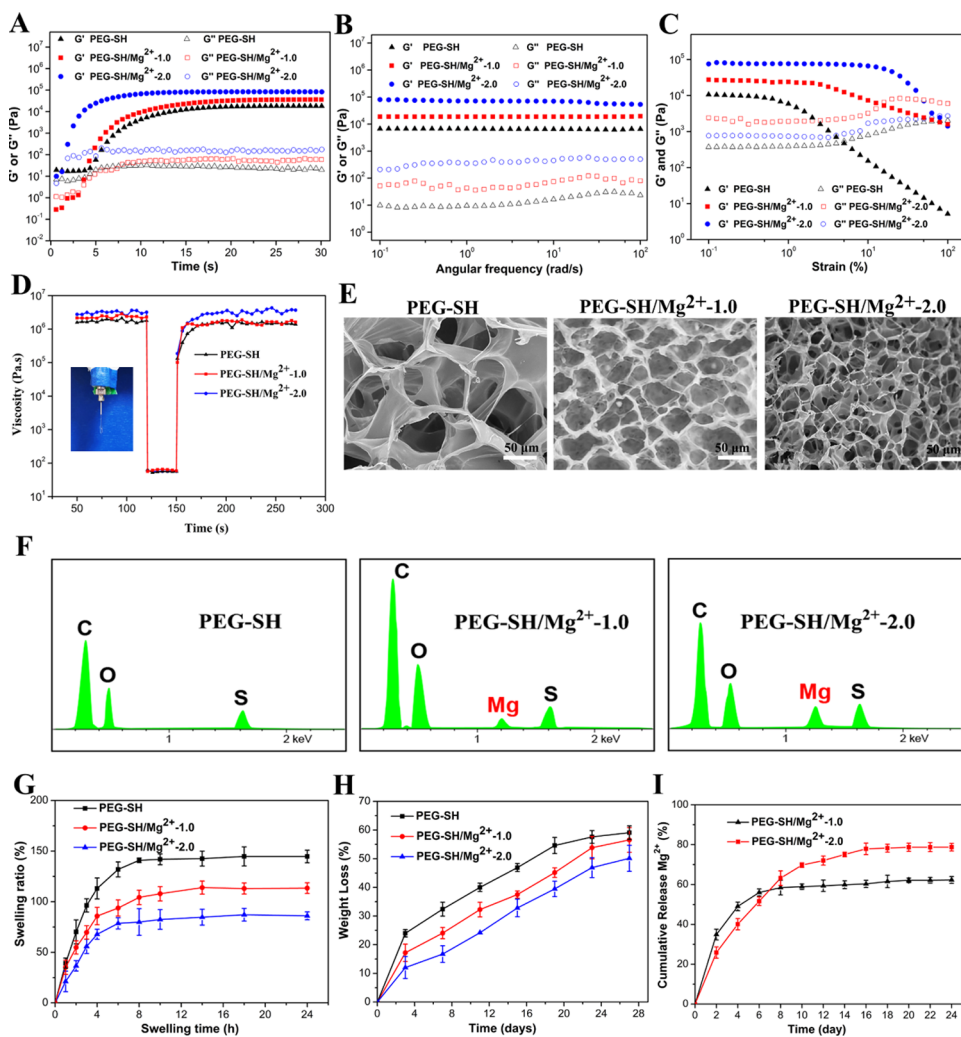


**Figure 2.** Rheological results of PEG-SH, PEG-SH/Mg<sup>2+</sup>-1.0, and PEG-SH/Mg<sup>2+</sup>-2.0 hydrogels: (A) time sweeping of storage modulus ( $G'$ ) and loss modulus ( $G''$ ) under a 50 mW/cm<sup>2</sup> UV irradiation, (B) frequency-dependent (at a strain of 1%) and (C) strain-dependent ( $\omega = 6.28$  rad/s) oscillatory shear, (D) measure of viscosity parameters in relation to time in seconds. The strain shearing rate alternated between 0.1% strain for 50 s and 100% strain for 25 s; (E) scanning electron microscopy (SEM) images of the cross-sectional interior structure of the hydrogels, (F) EDS analysis of samples, (G) swelling ratio and (H) degradation curves of resulting hydrogels in PBS solution at 37°C, and the (I) sustained release of Mg<sup>2+</sup> from PEG-SH/Mg<sup>2+</sup>-1.0 and PEG-SH/Mg<sup>2+</sup>-2.0 hydrogel systems.

rarely reported. Glycogen synthase kinase 3  $\beta$  (GSK3 $\beta$ ), an important PI3K/AKT signaling substrate, shows a regulatory role in mitochondrial activities.<sup>29</sup> The inhibition of GSK3 $\beta$  via its phosphorylation at Ser9 by activated PI3K/AKT signaling can cause  $\beta$ -catenin stabilization and its translocation into the nucleus for gene transcription.<sup>29–31</sup> Nevertheless, the specialized mechanisms underlying the regulation of bone defect repair by PI3K/AKT/GSK3 $\beta$ / $\beta$ -catenin signaling still remain to be elusive.

Herein, we reported injectable, Mg<sup>2+</sup> ion-rich hydrogels for bone defect regeneration. The resultant active hydrogel (PEG-SH/Mg<sup>2+</sup>) was produced through coordinative cross-linking based on 4-arm-thiolated polyethylene glycol (PEG-SH) and Mg<sup>2+</sup> ions. Because of the presence of dynamic and reversible nature of the Mg–S coordination bond, the Mg<sup>2+</sup> ion was gradually released from the hydrogel network. Such controllable slow-release Mg<sup>2+</sup> ion is particularly appealing for bone defect repair. The mechanical properties, rheology, morphology, swelling rate, and degradation behavior of the hydrogels were systematically studied. In addition, we investigated the cytocompatibility, differentiative behavior, and mechanism of

PEG-SH/Mg<sup>2+</sup> hydrogels in mesenchymal stem cells. As shown in Scheme 1, this study will provide a new carrier system with the sustained release of Mg<sup>2+</sup> to facilitate the proliferation and differentiation of bone marrow-derived mesenchymal stem cells (BMSCs) for regenerative medicine.

## 2. RESULTS AND DISCUSSION

**2.1. Preparation of PEG-SH/Mg<sup>2+</sup> Hydrogels and their Mechanical Properties.** Tissue engineering provides great opportunities to effectively promote bone regeneration, especially a multifunctional scaffold is a critical factor.<sup>32</sup> In this study, we used the bioactive Mg<sup>2+</sup> and biocompatible 4-arm-PEG-SH to prepare a Mg–S coordinative active hydrogel for bone tissue engineering (Figure 1A). As shown in Figure 1B, the mixed pregel solution can produce a transparent hydrogel via UV irradiation. The compression behaviors of fabricated hydrogels were analyzed to verify the influence of Mg<sup>2+</sup> on the mechanical properties. Obviously, the introduction of Mg<sup>2+</sup> increases the mechanical strength of PEG-based hydrogels. The PEG-SH/Mg<sup>2+</sup> hydrogel was prepared

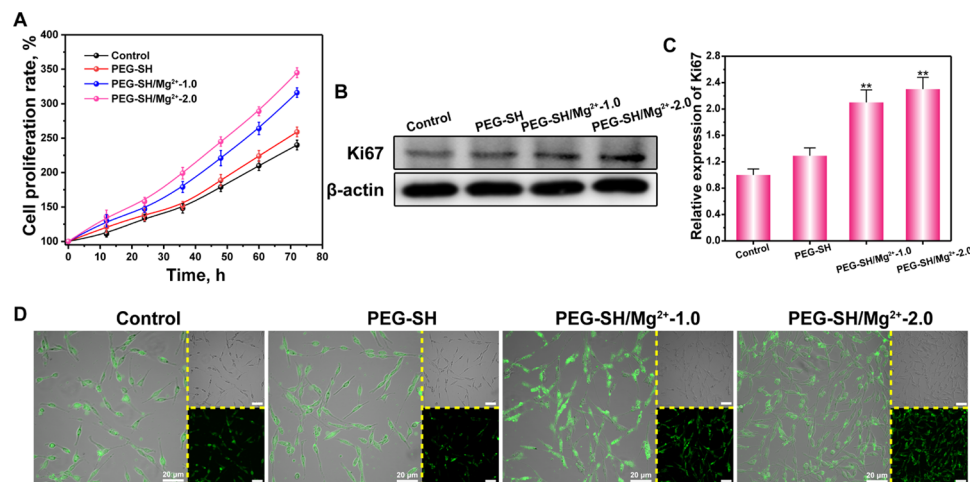


**Figure 3.** (A) Proliferation rate at 12, 24, 36, 48, 60, and 72 h; (B) western blot test of Ki67 protein expression and (C) statistical analysis of Ki67 expression of BMSCs cultured in PEG-SH, PEG-SH/Mg<sup>2+</sup>-1.0, and PEG-SH/Mg<sup>2+</sup>-2.0 hydrogels; (D) BMSC was stained by AO and observed by a fluorescence microscope. The values are represented as mean  $\pm$  standard deviation (SD) ( $n = 3$ ). \* $P < 0.05$  and \*\* $P < 0.01$  vs control. Scale bar is 20  $\mu$ m.

predominantly based on two mechanisms, the formation of a disulfide bond and coordination of Mg–S. The chemical structure of the obtained hydrogel was characterized by Fourier-transform infrared (FTIR) spectra to verify the formed mechanism of hydrogels. As shown in Figure 1C, a new peak appeared at about 530  $\text{cm}^{-1}$  in the PEG-SH sample and was attributed to the disulfide bond, whereas the corresponding peak in the PEG-SH/Mg<sup>2+</sup> hydrogel was not the focus because of the formation of a Mg–S coordinative hydrogel network. Thus, the compressive strength of the PEG-SH/Mg<sup>2+</sup> hydrogel significantly improved as the Mg<sup>2+</sup> content increased, and the PEG-SH/Mg<sup>2+</sup>-2.0 sample was 0.27 MPa higher than PEG-SH/Mg<sup>2+</sup>-1.0 (0.14 MPa), owing to the generation of Mg–S coordination bond leading to excellent mechanical performance. To comprehensively compare the mechanical performance of hydrogels, we evaluated their cyclic compressive behavior. During the process of 20 cycle compression measurements, the PEG-SH/Mg<sup>2+</sup>-1.0 and PEG-SH/Mg<sup>2+</sup>-2.0 specimens undergo the deformation of 60% without fracture (Figure 1D), and the narrow gap between the first compression/relaxation and last compression/relaxation curves of testing samples further demonstrated that they were compressible and reversible.

**2.2. Rheology Behavior, Micromorphology and Energy-Dispersive X-ray Spectroscopy (EDS) Analysis, Swelling Test, Weight Loss, and Mg<sup>2+</sup> Release Performance of PEG-SH/Mg<sup>2+</sup> Hydrogels.** To further reveal the mechanical properties of PEG-SH/Mg<sup>2+</sup> hydrogels, rheological measurements were conducted during the gelation process sequentially using time, frequency, and strain sweep. Figure 2A shows  $G'$  and  $G''$  of the pregels versus the sweep time. It is found that the gelation time of PEG-SH, PEG-SH/Mg<sup>2+</sup>-1.0, and PEG-SH/Mg<sup>2+</sup>-2.0 hydrogels was less than 5 s, which reflects the gelation kinetics of the polymer system. Due to different cross-linking mechanisms, the gelation time of the PEG-SH/Mg<sup>2+</sup> hydrogel is faster than that of the pure PEG-SH gel.

The results of frequency sweep of testing hydrogels are demonstrated in Figure 2B. The  $G'$  value remained constant over the entire frequency sweep range, indicating that the systems formed complete cross-linked network structures.<sup>32–34</sup>

As expected, the  $G'$  value of PEG-SH/Mg<sup>2+</sup>-2.0 was the highest, which was consistent with mechanical results. Strain-dependent oscillatory rheology (Figure 2C) of the PEG-SH/Mg<sup>2+</sup>-2.0 hydrogels presented a stress relaxation at strains over 50%, indicating a wide processing range and shear-thinning behavior. Afterwards, the continuous step strain approach was applied to perform the rheological recovery performance of the system. Figure 2D shows the hydrogel's ability to recover its structure under shear stress in a thixotropy test. Because of their shear-thinning property, hydrogels could be extruded through a needle without any clogging, indicating their good injectability. SEM images of lyophilized samples (Figure 2E) exhibited that the morphologies of three hydrogels were similar, whereas PEG-SH/Mg<sup>2+</sup> had a denser porous structure, owing to the formation of a uniform dense network structure via a disulfide bond and coordination of Mg and S. The interconnected porous structure of the hydrogel system is beneficial for the transmission of nutrients for cells, as well as capable of stimulating osteogenic differentiation of BMSCs.<sup>35</sup> EDS analysis (Figure 2F) showed substantial signals of the sulfur and magnesium at the SEM-observed locations of the samples, thereby proving the involvement of thiols and Mg<sup>2+</sup> in the formation of these structures.

The swelling property is determined by the water uptake capability of a hydrogel system. A smaller equilibrium swelling rate was observed in PEG-SH/Mg<sup>2+</sup>-1.0 and PEG-SH/Mg<sup>2+</sup>-2.0 groups (Figure 2H), which suggested that coordination between Mg and S formed a higher cross-linking network structure. A dense hydrogel system could hinder the movement of water molecules, leading to weak swelling behavior.<sup>36</sup> Appropriate degradation of the scaffolds was critical to support bone tissue regeneration.<sup>37</sup> Thus, we further assessed degradation performance of the hydrogel system in vitro by immersing in a PBS solution. As shown in Figure 2G, pure PEG-SH undergo higher degradation than PEG-SH/Mg<sup>2+</sup>-1.0 and PEG-SH/Mg<sup>2+</sup>-2.0 hydrogels. After soaking in PBS for 28 days, the weight loss of PEG-SH, PEG-SH/Mg<sup>2+</sup>-1.0, and PEG-SH/Mg<sup>2+</sup>-2.0 hydrogels were  $60.9 \pm 0.7$ ,  $56.4 \pm 0.4$ , and  $50.2 \pm 1.6\%$ , respectively. Obviously, the Mg<sup>2+</sup> introduced to the polymer system exhibited a decreasing degradation, which is likely attributed to the higher cross-link

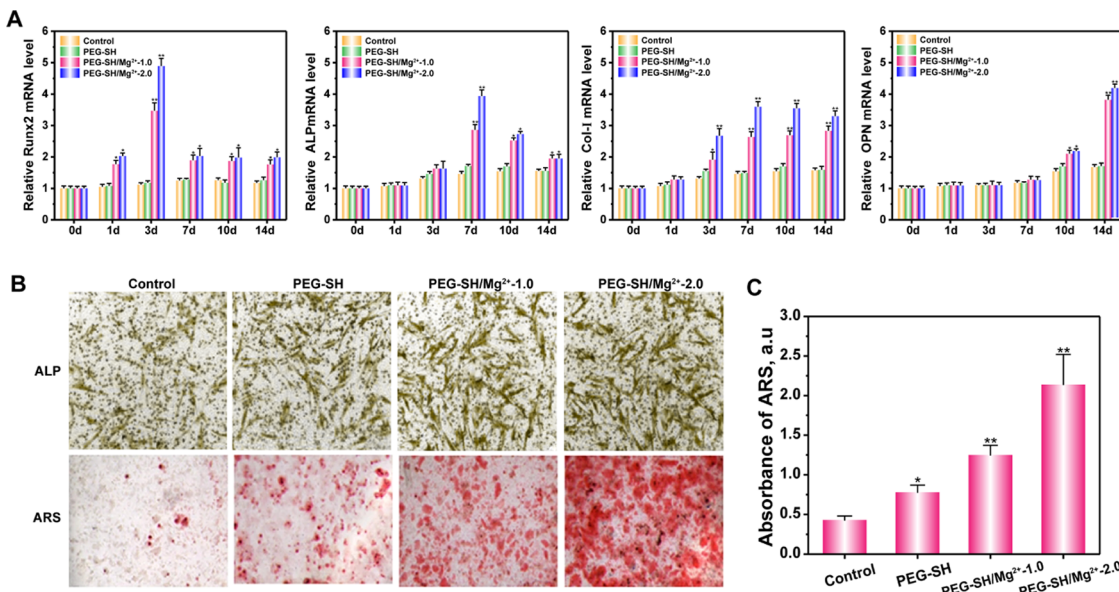


**Figure 4.** (A) Evaluating osteogenic differentiation of BMSCs cultured on the PEG-SH/ $Mg^{2+}$  hydrogel by analyzing relative expressions of genes in relation to osteogenic differentiation: Runx2 gene; ALP gene; COL-I gene; OPN gene at 0, 1, 3, 7, 10, and 14 days; (B) microscopic images of ALP staining and alizarin red staining assays; (C) quantitative mineralization of BMSCs cocultured with PEG-SH, PEG-SH/ $Mg^{2+}$ -1.0, and PEG-SH/ $Mg^{2+}$ -2.0 at day 14. The values are represented as mean  $\pm$  SD ( $n = 3$ ). \* $P < 0.05$  and \*\* $P < 0.01$  vs control.

density and therapy, resulting in a more stable polymer structure.

Although  $Mg^{2+}$  has been previously reported to be used in bone tissue engineering, the burst and excessive release of  $Mg^{2+}$  from a carrier platform may actually cause bone loss. Therefore, the site-specific controlled release of  $Mg^{2+}$  from the delivery vehicles is highly appealing but challenging. Herein, we estimated the release behavior of  $Mg^{2+}$  from PEG-SH/ $Mg^{2+}$ -1.0 and PEG-SH/ $Mg^{2+}$ -2.0 hydrogels incubated in PBS (Figure 2I). Compared to the PEG-SH/ $Mg^{2+}$ -1.0 hydrogels, the PEG-SH/ $Mg^{2+}$ -2.0 group featured clearly smaller initial burst release and slower subsequent release of  $Mg^{2+}$  within 7 days. After incubation of 24 days, about 80% of  $Mg^{2+}$  was released from the PEG-SH/ $Mg^{2+}$ -2.0 sample in a continuous manner, which was higher than that of PEG-SH/ $Mg^{2+}$ -1.0 (approximately 60%) over the same period. The denser coordination between the Mg and S of hydrogel structure can be regarded as a barrier to prevent the  $Mg^{2+}$  release rate and lead to more stability and sustained release in 24 days, which showed better release results of  $Mg^{2+}$  than reported by Kang et al. for a Mg-enriched system.<sup>38</sup> All of these in vivo evaluation results indicated that PEG-SH/ $Mg^{2+}$ -2.0 hydrogels with the sustained release of  $Mg^{2+}$  have a great prospect for stimulating the osteogenesis of stem cells.

**2.3. Effects of the PEG-Mg<sup>2+</sup> Hydrogel on Proliferation in BMSCs.** Figure 3 shows the proliferation of BMSC cells cultured with PEG-SH, PEG-SH/ $Mg^{2+}$ -1.0, and PEG-SH/ $Mg^{2+}$ -2.0 hydrogel samples. The proliferation curve, as shown in Figure 3A, indicates that PEG-SH/ $Mg^{2+}$ -2.0 has greater cell proliferation viability than both PEG and PEG-SH/ $Mg^{2+}$ -1.0 groups at 72 h. This demonstrates that  $Mg^{2+}$  is biologically friendly and owns the ability to promote proliferation in a dose-dependent manner. To further confirm the result of cell viability, the Ki67 expression of BMSCs cultured with the response to samples were tested using western blot. Ki67 is a proliferation-related antigen, which is closely related to mitosis, and is indispensable in cell

proliferation.<sup>39</sup> Thus, ki67 is mainly used to evaluate cell proliferation in clinics. As shown in Figure 3B,C, the PEG-SH/ $Mg^{2+}$ -2.0 group shows greater expression of Ki67 than the other groups. To more intuitively display the growth and proliferation of cells, BMSCs were stained by acridine orange (AO).<sup>40</sup> AO can penetrate the intact membranes and get embedded in the nuclear DNA to make cells emit a bright green light. As shown in Figure 3D, the PEG-SH/ $Mg^{2+}$ -2.0 group shows the largest number of cells than the other groups. Overall, the PEG-SH/ $Mg^{2+}$  hydrogel can promote proliferation due to the effect of  $Mg^{2+}$ .

**2.4. Effects of the PEG-SH/ $Mg^{2+}$  Hydrogel on Differentiation and Osteogenesis in BMSCs.** To investigate the role of the PEG-SH/ $Mg^{2+}$ -2.0 hydrogel in the regulation of BMSC differentiation and osteogenesis, the quantitative polymerase chain reaction (qPCR) was carried out on days 0, 1, 3, 7, 10, and 14. Several typical mRNA expression levels of the bone markers including Runx2, Col-I, ALP, and OPN were significantly promoted by the  $Mg^{2+}$  content (Figure 4A). Runx2 is the very early maker of osteogenesis differentiation, and it usually lasts only a few days. Obviously, the Runx2 mRNA expression was the highest at day 3 and as time progressed, the expression decreased to a relatively stable value. ALP presents an early osteogenic marker, which can reflect the differentiation activity. The expression of ALP mRNA showed a significant difference between the PEG-SH/ $Mg^{2+}$ -2.0 group and the other groups at day 7. Type I collagen is the most important fibrous collagen component in the bone matrix, with specificity and is an important indicator reflecting osteogenesis. Similarly, the Col-I mRNA expression of the PEG-SH/ $Mg^{2+}$ -2.0 group was significantly higher than other groups at day 3 and maintained a relatively high level. The consistently high expression of Col-I mRNA is a benefit for bone mineralization. Moreover, OPN (osteopontin) is an osteogenic marker for osteoblastic mineralization and maturation. As can be seen, the OPN mRNA expression of PEG-SH/ $Mg^{2+}$ -1.0 and PEG-SH/ $Mg^{2+}$ -2.0 groups became higher than

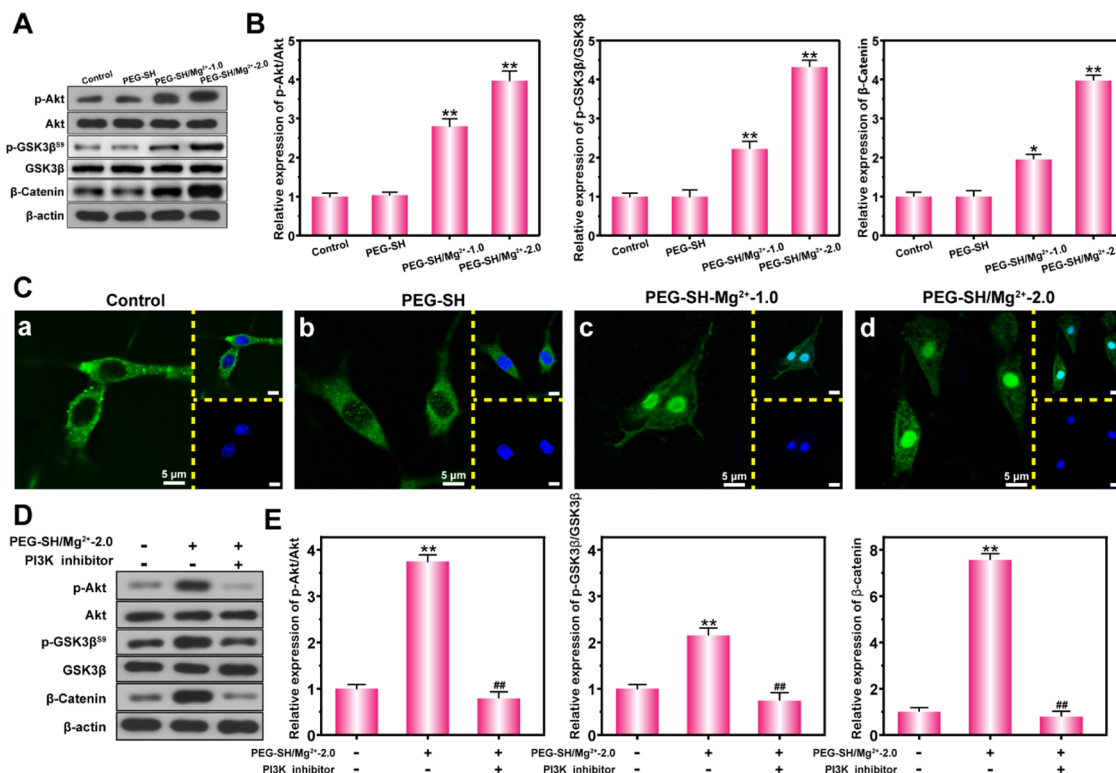


**Figure 5.**  $Mg^{2+}$ -activated BMSC PI3K/AKT/GSK3 $\beta$ /β-catenin signaling in the PEG-SH/ $Mg^{2+}$  hydrogel coculture system at day 3. (A) Western blot images and (B) statistical analysis showing the expression of p-AKT/AKT, p-GSK3 $\beta$ /GSK3 $\beta$ , and β-Catenin in BMSCs; (C) immunofluorescence analysis of the distribution of β-catenin (green) in BMSCs; (D) expression of p-AKT/AKT, p-GSK3 $\beta$ /GSK3 $\beta$ , and β-catenin altered by the PI3K inhibitor was detected using western blotting in BMSCs and (E) its corresponding statistical analysis. The values are represented as mean  $\pm$  SD ( $n = 3$ ). \* $P < 0.05$  and \*\* $P < 0.01$  vs control; # $P < 0.05$  and ## $P < 0.01$  vs PEG-SH/ $Mg^{2+}$ -2.0.

the other groups at 14 day. ALP and ARS staining were also conducted to generally assess the effect of PEG-SH/ $Mg^{2+}$  on ALP activity and mineralization of the extracellular matrix (ECM). The corresponding results (Figure 4B) staining performed on day 7 showed that the PEG-SH/ $Mg^{2+}$ -2.0 group significantly enhanced both ALP activity and calcium deposition. The semiquantitative ARS analysis showed that the PEG-SH/ $Mg^{2+}$ -2.0 sample was 4.98-fold, 2.74-fold, and 1.71-fold greater than the control, PEG-SH, and PEG-SH/ $Mg^{2+}$ -1.0 groups (Figure 4C). Thus, the expression levels of bone markers were increased by the stimulation of the  $Mg^{2+}$  ion.

**2.5. Mechanism of Promoting BMSC Differentiation by the PEG-SH/ $Mg^{2+}$  Hydrogel.** To investigate the mechanism related to the functions of promoting osteogenic differentiation by the PEG-SH/ $Mg^{2+}$  hydrogel, we performed western blot analysis of PI3K/AKT and Wnt signaling pathway-related proteins expression. As shown in Figure 5A,B, the PEG-SH/ $Mg^{2+}$ -2.0 group increased the expression level of phosphorylated AKT (Ser473) and GSK3 $\beta$  (Ser9), meanwhile the expression of β-catenin was also enhanced. Additionally, as shown in Figure 5C, the nuclear localization of β-catenin (green) was more pronounced in PEG-SH/ $Mg^{2+}$ -1.0 and PEG-SH/ $Mg^{2+}$ -2.0 groups. However, β-catenin was more pronounced in the cytoplasm in the control and PEG-SH groups. These findings reveal that the Wnt/β-catenin signaling pathway is also an important signaling pathway during the differentiation and proliferation of bone cells.

Therefore, the western blot test and β-catenin immunofluorescence localization results demonstrated that the PEG-SH/ $Mg^{2+}$ -2.0 hydrogel could promote differentiation via

PI3K/AKT/GSK3 $\beta$ /β-catenin signaling. To further verify the differentiation mechanism of the PEG-SH/ $Mg^{2+}$ -2.0 hydrogel through the PI3K/AKT/GSK3 $\beta$  signaling pathway, we introduced the PI3K inhibitor. As shown in Figure 5D and E, the expression of p-Akt, p-GSK3 $\beta$ , and β-catenin decreased with the addition of the PI3K inhibitor. The experiment result proved that the β-catenin/Wnt signaling pathway was activated by the PI3K/AKT/GSK3 $\beta$  signaling pathway. This result is consistent with the previously reported; the PI3K/AKT pathway modulates many cellular functions through the inhibition of GSK3 $\beta$  (phosphorylated at position Ser9), which allows β-catenin to stabilize and translocate into the nucleus for gene transcription.<sup>29,30,41</sup> In summary, the PEG-SH/ $Mg^{2+}$  hydrogel could promote the differentiation via the PI3K/Akt/GSK3 $\beta$ /β-catenin signal pathway.

### 3. CONCLUSIONS

In this study, a PEG-SH/ $Mg^{2+}$  hydrogel system was prepared for the sustained release of  $Mg^{2+}$  ions to facilitate the BMSC proliferation and differentiation. Such active hydrogels are stabilized by the multivalent cross-linking domains formed by a dynamic nature coordination bond of Mg–S and a dynamic disulfide bond of S–S, and the therapy feature enhanced the mechanical strength, capacity for injectability, stabilized swelling, and degradation performance. Due to the dynamic nature coordination bond of Mg–S and the dynamic disulfide bond of S–S, the designed PEG-SH/ $Mg^{2+}$  system showed sustained local delivery of bioactive magnesium ions into the surrounding environment for BMSC proliferation and differentiation via the PI3K/Akt/GSK3 $\beta$ /β-catenin signal pathway.

All of these promising results indicate that the coordinative cross-linking PEG-SH/Mg<sup>2+</sup> hydrogel is particularly appealing for magnesium ion delivery applications to stimulate bone regeneration.

#### 4. MATERIALS AND METHODS

**4.1. Fabrication of PEG-SH/Mg<sup>2+</sup> Hydrogels.** First, 4-arm-PEG-SH (600 mg,  $M_w = 20\,000$ , purchased from Sigma-Aldrich,) was dissolved in water (1 mL). Then, 400  $\mu\text{L}$  of an aqueous solution of MgCl<sub>2</sub> was diluted in 600  $\mu\text{L}$  of deionized water. Each aqueous solution was placed in two separate tubes. Upon mixing, the pregel solution formed transparent gels with 0.1 and 0.2 M of Mg<sup>2+</sup> after 60 s of UV irradiation (50 mW/cm<sup>2</sup>, 365 nm), which was named as PEG-SH/Mg<sup>2+</sup>-1.0 and PEG-SH/Mg<sup>2+</sup>-2.0 respectively, and then was washed with a PBS solution. The pure PEG-SH hydrogel was also prepared using the same method. The FTIR spectra of PEG-SH and PEG-SH/Mg<sup>2+</sup> hydrogel samples were conducted on a Nicolet 6700 FTIR spectrometer (Thermo Scientific).

**4.2. Mechanical Property Tests.** The compressive stress-strain tests of hydrogels were conducted at room temperature using a universal mechanical testing machine (AGI-1, Shimaodzu, 1 KN load, Japan) with the capacity of 100 N. Hydrogel samples were put in a cylinder with a 10 mm diameter and a 8 mm height. The specimens were compressed to 70% strain with a deformation rate of 1 mm/min. Then, the cycling compression experiment was performed at a constant strain speed of 2 mm/min up to 60% strain and then recovered to 0% strain with the same rate, and the cycle was repeated for 20 times.

**4.3. Rheological, Scanning Electron Microscopy (SEM), and Energy-Dispersive X-ray Spectroscopy (EDS) Analyses.** The rheological properties of hydrogels were determined on an rotational rheometer (DHR, TA Instruments) equipped with a UV-irradiated instrument (OmniCure S2000) at 37 °C. First, the gelation time of the PEG-SH and PEG-SH/Mg<sup>2+</sup> pregel solutions was studied via time sweeps (oscillatory strain of 1% and a frequency of 6.28 rad/s) under UV irradiation. Then, the frequency sweep oscillatory tests were performed at a constant strain of 1% by varying amplitude frequency 0.1 to 100 rad/s. Finally, the strain sweep was carried out to confirm that this modulus value was within the linear elastic regime (frequency of 6.28 rad/s and oscillatory strain from 0.1% to 100%), and the step strain test was constructed by a hydrogel scaffold subjected to a low strain ( $\gamma = 0.1\%$ ) during the first 50 s, followed by a high strain ( $\gamma = 100\%$ ) during the next 25 s. Three replicates were performed for all experiments.

To study the inner structure of the obtained hydrogel samples, all lyophilized specimens were mounted onto copper studs and sputter-coated with gold/palladium for 60 s. Then, a field-emission scanning electron microscope (FE-SEM, ULTRA 55, Carl Zeiss, Germany) equipped with an energy-dispersive spectrometry (EDS) system was used to determine the morphology and element component and contents of the response to the hydrogel.

**4.4. Equilibrium Swelling Rate, Degradation, and In Vitro Mg<sup>2+</sup> Release Studies.** A swelling test was used to estimate the swelling ratio (SR) and the stability of the hydrogels. The obtained hydrogel specimens were put into 20 mL of PBS (0.01 M pH 7.4) in sealed vials at 37°C. When reaching the preset time interval, the hydrogels were taken out from the solution and weighed after absorbing the excess

surface water with a filter paper. The test was not finished until the weight of hydrogel testing samples remained constant. SR was calculated using the following equation: SR =  $(W_t - W_i)/W_i$ , where  $W_i$  and  $W_t$  represent the initial weight of the hydrogels and the weight after swelling equilibrium, respectively. Three replicates were performed for all experiments.

As for the degradation performance of fabricated samples, the initial weight of each sample was recorded ( $W_0$ ). After that, the hydrogels were placed into a PBS solution and the hydrogels were taken up, washed with water, lyophilized, and weighed again ( $W_T$ ) at timed intervals. The study was conducted in a 37°C shaker for 26 days. The weight loss =  $(W_0 - W_T)/W_0 \times 100\%$ .

The release evaluation was conducted to investigate the release behavior of Mg<sup>2+</sup> loaded in the PEG-SH/Mg<sup>2+</sup>-1.0 or PEG-SH/Mg<sup>2+</sup>-2.0 polymer network; the hydrogel samples were incubated in a testing tube with 1 mL of PBS buffer. Subsequently, 100  $\mu\text{L}$  of the supernatant was collected at a specified time and followed by the addition of an equal volume of fresh PBS. The supernatant samples were analyzed by a magnesium colorimetric assay kit.

**4.5. BMSC Isolation, Cultivation, and Identification.** BMSCs were isolated from the femur and tibia of Sprague Dawley (SD) rats.<sup>42</sup> (4 weeks old, weighing 50–65 g). After the osteoepiphysis was removed, the bone marrow tissue was flushed out from the femur and tibia by a DMEM complete medium. The marrow was repeatedly pipetted for obtaining a homogeneous cell suspension. Then, the cell suspension was seeded in a 25 cm<sup>2</sup> cell culture flask and incubated in a humid atmosphere at 37 °C with 5% CO<sub>2</sub>. The medium was changed every two days and the remaining adherent cells (defined as BMSCs) were digested by 0.25% trypsin EDTA solution until they reached 90% confluence. For identification, BMSCs were digested with 0.25% trypsin and washed using PBS containing bovine serum albumin (BSA, 20%). The cells were subsequently resuspended in a complete medium to a single-cell suspension at a density of  $5 \times 10^6$  cells/mL. Eppendorf tubes were used to contain the single cell suspension and each tube was filled with 200  $\mu\text{L}$  of the suspension ( $5 \times 10^6$  cells/mL). Rat antimouse antibodies against CD29 (FITC-conjugated), CD34 (FITC-conjugated), CD44 (phycoerythrin-conjugated), CD45 (phycoerythrin-conjugated), and fluorescein isothiocyanate-labeled mouse IgG (BD Biosciences, Franklin Lakes, NJ) for flow cytometric observation were added to the EP tubes, incubated at 4 °C for 60 min, washed by sterilized PBS three times, resuspended following centrifugation at 120 g at 4 °C for 5 min, and fixed with 200  $\mu\text{L}$  of polyoxymethylene (4%) at 4 °C for 1 h. A flow cytometer and Cell-Quest software (version 5.1; BD Biosciences) were used to determine their cell phenotype.

**4.6. BMSC Proliferation.** The 96-well cell culture plate bottom was injected with 100  $\mu\text{L}$  of 4-arm-PEG-SH and MgCl<sub>2</sub> mixed solution. The plates were placed onto shaker (HZ150L, Wuhan Ruihua Co., LTD.) at 100 rpm. The experimental group was control (without the hydrogel), PEG-SH, PEG-SH/Mg<sup>2+</sup>-1.0, and PEG-SH/Mg<sup>2+</sup>-2.0 groups, respectively. After 1 min of mixing, the two solutions formed transparent gels for detecting the BMSC proliferation. Then, BMSCs ( $1 \times 10^4$  cells per well) were seeded and cultivated in a 96-well plate for 12, 24, 36, 48, 60, and 72 h, and 20  $\mu\text{L}/\text{well}$  of MTT solution (5 mg mL<sup>-1</sup> in PBS) was added into each well. Then, the culture medium was removed and replaced with 150

**Table 1.** Primers for qRT-PCR Analysis of Gene Expression

primer	5' forward 3'	5' reverse 3'
Runx2	TACTGTCATGGCGGGTAACG	CACCTGCCTGGCTCTTCTTA
ALP	CAAGGATGCTGGGAAGTCGG	CTCTGGGCGCATCTCATTGT
Col-I	GGAGACGGCTATTTGGACG	TCCCTGAGTGGAGCTTCAT
OPN	GAACATGAAATGCTCTTCAG	TCCATGAAGCCACAAACTAAACTA
$\beta$ -Actin	GCTTCTAGGCAGTGTAC	CCATGCCAATGTTGTCTCTT

$\mu\text{L}$ /well of DMSO after incubation for 4 h. The real-time data was determined at 570 nm using a microplate reader. The proliferative marker Ki67 was detected using western blot at 72 h. The detailed steps of WB are listed below. Additionally, 50  $\mu\text{L}$  of acridine orange (diluted concentration 1:100) was added into the 96-well cell culture plate to observe BMSC growth situation at 72 h.

**4.7. PEG-SH/Mg<sup>2+</sup> Hydrogel Promoted the BMSC Differentiation Mechanism.** Immunofluorescence (IF) assay: BMSCs were cultured in a 96-well plate with the hydrogel at the bottom. The experiment was divided into four groups: control, PEG-SH, PEG-SH/Mg<sup>2+</sup>-1.0, and PEG-SH/Mg<sup>2+</sup>-2.0 groups, respectively. Cells were fixed with 4% paraformaldehyde and then permeabilized with 0.05% Triton X-100 for 1–2 min. Next, cells were blocked with 5% BSA for 1 h and incubated with the following anti- $\beta$ -catenin antibodies (ab16051) overnight at 4 °C. Subsequently, the species-matched secondary antibody antimouse Alexa Fluor 488 (1:400) was used, and the nucleus was stained with 4',6-diamidino-2-phenylindole (DAPI). The photographs were acquired with a confocal microscope (Zeiss LSM 880, Germany).

To verify the differentiation mechanism of Mg<sup>2+</sup> via the PI3K signal pathway, a PI3K inhibitor (LY294002) was introduced. The cells were seeded on the hydrogel in a 96-well plate and were divided into three groups according to the type of the bottom hydrogel: control (without the hydrogel), PEG-SH/Mg<sup>2+</sup>-1.0, and PEG-SH/Mg<sup>2+</sup>-2.0. After culturing for 72 h, the PI3K/ $\beta$ -catenin signal pathway was detected by western blot.

**4.8. ALP and Alizarin Red Staining.** Alizarin red staining and ALP staining were applied to study the ability of mineral deposition of BMSCs. The cell culture plates with the hydrogel at the bottom seeded with BMSCs were fixed with 4% paraformaldehyde and stained with 0.1% alizarin red and an ALP detection kit after 14 days of culture. Meanwhile, the quantitative analysis was also evaluated using an automatic microplate reader (Thermo Scientific) at 570 nm.<sup>43</sup>

**4.9. Western Blot Analysis.** In western blotting analysis, the total protein (20  $\mu\text{g}$ ) was separated by electrophoresis on 10% SDS-PAGE and then transferred onto nitrocellulose membranes by electroblotting. After that, the membranes were blocked with 5% nonfat dry milk in Tris-buffered saline with Tween 20 (TBST) and incubated with the primary antibody overnight at 4 °C. Immunolabeling was observed using an ECL reagent (Thermo Fisher Scientific). The antibodies employed for western blot were from the following sources: anti-p-Akt antibody (Abcam, ab8805), anti-Akt antibody (Abcam, ab18785), anti-GSK3  $\beta$  (phospho S9) antibody (Abcam, ab131097), anti-GSK3  $\beta$  antibody (ab131356), anti- $\beta$ -Catenin antibody (ab32572), anti-Ki67 antibody (Abcam, ab23878), and PI3K inhibitor (GDC-0941, ab141352).

**4.10. RT-qPCR.** Total RNA was isolated from BMSCs using an ultrapure RNA kit (CWBIOM, China) following the

manufacturer's instructions, and reverse transcribed into a first-strand complementary DNA (cDNA) by a PrimeScript RT reagent Kit (Takara). Amplification reactions were set up in a 96-well plate using iTaq SYBR Green Super mix (BIO-RAD), to which gene-specific forward and reverse PCR primers were added. These analyses were performed to detect Runx2, ALP, Col-I, and OPN mRNA expression, and  $\beta$ -actin was used as an internal control. The primer sequences are listed in Table 1.

## AUTHOR INFORMATION

### Corresponding Authors

Wenqiang Li – Department of Rehabilitation Medicine, Dapeng New District Nan'ao People's Hospital, Shenzhen 518121, China; Engineering Technology Research Center for Sports Assistive Devices of Guangdong, Guangzhou Sport University, Guangzhou 510000, China; [orcid.org/0000-0002-1498-2258](https://orcid.org/0000-0002-1498-2258); Email: [405119923@qq.com](mailto:405119923@qq.com)

Weiyi Pan – Department of Rehabilitation Medicine, Dapeng New District Nan'ao People's Hospital, Shenzhen 518121, China; Email: [sportsp@163.com](mailto:sportsp@163.com)

Yulong Wang – Department of Rehabilitation Medicine, Dapeng New District Nan'ao People's Hospital, Shenzhen 518121, China; Department of Rehabilitation, The Second People's Hospital of Shenzhen, The First Affiliated Hospital of Shenzhen University, Shenzhen 518035, China; Email: [wangyulong@szu.edu.cn](mailto:wangyulong@szu.edu.cn)

### Authors

Jiayu Liu – Department of Rehabilitation Medicine, Dapeng New District Nan'ao People's Hospital, Shenzhen 518121, China

Hongli Zeng – Department of Pediatric Rehabilitation, The Women and Children's Hospital of Dapeng New District, Shenzhen 518000, China

Peng Xiao – Department of Rehabilitation Medicine, Dapeng New District Nan'ao People's Hospital, Shenzhen 518121, China

Anqun Yang – Department of Rehabilitation Medicine, Dapeng New District Nan'ao People's Hospital, Shenzhen 518121, China

Xingxian Situ – Department of Rehabilitation Medicine, Dapeng New District Nan'ao People's Hospital, Shenzhen 518121, China

Yao Wang – Department of Rehabilitation Medicine, Dapeng New District Nan'ao People's Hospital, Shenzhen 518121, China

Xiang Zhang – Department of Rehabilitation Medicine, Dapeng New District Nan'ao People's Hospital, Shenzhen 518121, China

Complete contact information is available at:

<https://pubs.acs.org/10.1021/acsomega.0c02946>

### Notes

The authors declare no competing financial interest.

## ACKNOWLEDGMENTS

This work was supported by the Sanming Project of Medicine in Shenzhen (SZSM201610039) and Information Technology of Shenzhen (201806081018272960).

## REFERENCES

- (1) Mehta, M.; Schmidt-Bleek, K.; Duda, G. N.; Mooney, D. J. Biomaterial delivery of morphogens to mimic the natural healing cascade in bone. *Adv. Drug Delivery Rev.* **2012**, *64*, 1257–1276.
- (2) Kokubo, T.; Kim, H.-M.; Kawashita, M. Novel bioactive materials with different mechanical properties. *Biomaterials* **2003**, *24*, 2161–2175.
- (3) Shin, H.; Jo, S.; Mikos, A. G. J. B. Biomimetic materials for tissue engineering. *Biomaterials* **2003**, *24*, 4353–4364.
- (4) Ferreira, A.; Gentile, P.; Chiono, V.; Ciardelli, G. Collagen for bone tissue engineering. *Acta Biomater.* **2012**, *8*, 3191–3200.
- (5) Zhao, C.; Qazvini, N. T.; Sadati, M.; Zeng, Z.; Huang, S.; De La Lastra, A. L.; Zhang, L.; Feng, Y.; Liu, W.; Huang, B.; et al. A pH-Triggered, Self-Assembled, and Bioprintable Hybrid Hydrogel Scaffold for Mesenchymal Stem Cell Based Bone Tissue Engineering. *ACS Appl. Mater. Interfaces* **2019**, *11*, 8749–8762.
- (6) Heo, D. N.; Hospodiuk, M.; Ozbolat, I. T. Synergistic interplay between human MSCs and HUVECs in 3D spheroids laden in collagen/fibrin hydrogels for bone tissue engineering. *Acta Biomater.* **2019**, *95*, 348–356.
- (7) Makvandi, P.; Ali, G. W.; Della Sala, F.; Abdel-Fattah, W. I.; Borzacchiello, A. Hyaluronic acid/corn silk extract based injectable nanocomposite: A biomimetic antibacterial scaffold for bone tissue regeneration. *Mater. Sci. Eng.: C* **2020**, *107*, No. 110195.
- (8) Hutmacher, D. W. Scaffold design and fabrication technologies for engineering tissues—state of the art and future perspectives. *J. Biomater. Sci., Polym. Ed.* **2001**, *12*, 107–124.
- (9) Stratton, S.; Shelke, N. B.; Hoshino, K.; Rudraiah, S.; Kumbar, S. G. Bioactive polymeric scaffolds for tissue engineering. *Bioactive Mater.* **2016**, *1*, 93–108.
- (10) Zhai, X.; Ruan, C.; Ma, Y.; Cheng, D.; Wu, M.; Liu, W.; Zhao, X.; Pan, H.; Lu, W. W. J. A. S. 3D-Bioprinted Osteoblast-Laden Nanocomposite Hydrogel Constructs with Induced Microenvironments Promote Cell Viability, Differentiation, and Osteogenesis both In Vitro and In Vivo. *Adv. Sci.* **2018**, *5*, No. 1700550.
- (11) Staiger, M. P.; Pietak, A. M.; Huadmai, J.; Dias, G. Magnesium and its alloys as orthopedic biomaterials: A review. *Biomaterials* **2006**, *27*, 1728–1734.
- (12) Kim, B.-S.; Kim, J. S.; Park, Y. M.; Choi, B.-Y.; Lee, J. Mg ion implantation on SLA-treated titanium surface and its effects on the behavior of mesenchymal stem cell. *Mater. Sci. Eng.: C* **2013**, *33*, 1554–1560.
- (13) Witte, F.; Kaese, V.; Haferkamp, H.; Switzer, E.; Windhagen, H. J. B. In vivo corrosion of four magnesium alloys and the associated bone response. *Biomaterials* **2005**, *26*, 3557–3563.
- (14) Yoshizawa, S.; Brown, A.; Barchowsky, A.; Sfeir, C. J. A. b. Magnesium ion stimulation of bone marrow stromal cells enhances osteogenic activity, simulating the effect of magnesium alloy degradation. *Acta Biomater.* **2014**, *10*, 2834–2842.
- (15) Yang, J.; Wu, Y.; Shen, Y.; Zhou, C.; Li, Y.-F.; He, R.-R.; Liu, M. Enhanced therapeutic efficacy of doxorubicin for breast cancer using chitosan oligosaccharide-modified halloysite nanotubes. *ACS Appl. Mater. Interfaces* **2016**, *8*, 26578–26590.
- (16) Yuan, Z.; Wei, P.; Huang, Y.; Zhang, W.; Chen, F.; Zhang, X.; Mao, J.; Chen, D.; Cai, Q.; Yang, X. J. A. b. Injectable PLGA microspheres with tunable magnesium ion release for promoting bone regeneration. *Acta Biomater.* **2019**, *85*, 294–309.
- (17) Zhang, K.; Feng, Q.; Xu, J.; Xu, X.; Tian, F.; Yeung, K. W. K.; Bian, L. Self-Assembled Injectable Nanocomposite Hydrogels Stabilized by Bisphosphonate-Magnesium ( $Mg^{2+}$ ) Coordination Regulates the Differentiation of Encapsulated Stem Cells via Dual Crosslinking. *Adv. Funct. Mater.* **2017**, *27*, No. 1701642.
- (18) Zhang, K.; Jia, Z.; Yang, B.; Feng, Q.; Xu, X.; Yuan, W.; Li, X.; Chen, X.; Duan, L.; Wang, D.; Bian, L. Adaptable Hydrogels Mediate Cofactor-Assisted Activation of Biomarker-Responsive Drug Delivery via Positive Feedback for Enhanced Tissue Regeneration. *Adv. Sci.* **2018**, *5*, No. 1800875.
- (19) Jiang, X.; Wang, G.; Li, J.; Zhang, W.; Xu, L.; Pan, H.; Jin, W.; Liu, X.; Wu, Q.; Jiao, T. J. I. J. N. Magnesium ion implantation on a micro/nanostructured titanium surface promotes its bioactivity and osteogenic differentiation function. *Int. J. Nanomed.* **2014**, *9*, 2387–2398.
- (20) Hung, C.-C.; Chaya, A.; Liu, K.; Verdelis, K.; Sfeir, C. J. A. b. The role of magnesium ions in bone regeneration involves the canonical Wnt signaling pathway. *Acta Biomater.* **2019**, *98*, 246–255.
- (21) Zhang, L.; Yang, C.-x.; He, S.-s. Recent advances in the study of regulation effect of TRPM family in cellular calcium/magnesium homeostasis. *Basic Clin. Med.* **2013**, *3*, 371–373.
- (22) Díaz-Tocados, J. M.; Herencia, C.; Martínez-Moreno, J. M.; de Oca, A. M.; Rodríguez-Ortiz, M. E.; Vergara, N.; Blanco, A.; Steppan, S.; Almadén, Y.; Rodríguez, M. Magnesium Chloride promotes Osteogenesis through Notch signaling activation and expansion of Mesenchymal Stem Cells. *Sci. Rep.* **2017**, *7*, No. 7839.
- (23) de Oca, A. M.; Guerrero, F.; Martínez-Moreno, J. M.; Madueno, J. A.; Herencia, C.; Peralta, A.; Almaden, Y.; Lopez, I.; Aguilera-Tejero, E.; Gundlach, K. Magnesium inhibits Wnt/ $\beta$ -catenin activity and reverses the osteogenic transformation of vascular smooth muscle cells. *PLoS One* **2014**, *9*, No. e89525.
- (24) Qi, T.; Weng, J.; Yu, F.; Zhang, W.; Li, G.; Qin, H.; Tan, Z.; Zeng, H. Insights into the Role of Magnesium Ions in Affecting Osteogenic Differentiation of Mesenchymal Stem Cells. *Biol. Trace Elem. Res.* **2020**, *1*–9.
- (25) Ciccarello, M.; Zini, R.; Rossi, L.; Salvestrini, V.; Ferrari, D.; Manfredini, R.; Lemoli, R. Extracellular Purines Promote the Differentiation of Human Bone Marrow-Derived Mesenchymal Stem Cells to the Osteogenic and Adipogenic Lineages. *Stem Cells Dev.* **2013**, *22*, 1097–1111.
- (26) Liu, L.; Xiang, Y.; Wang, Z.; Yang, X.; Yu, X.; Lu, Y.; Deng, L.; Cui, W. Adhesive liposomes loaded onto an injectable, self-healing and antibacterial hydrogel for promoting bone reconstruction. *NPG Asia Mater.* **2019**, *11*, No. 81.
- (27) Wang, J.; Ma, X. Y.; Feng, Y. F.; Ma, Z. S.; Ma, T. C.; Zhang, Y.; Li, X.; Wang, L.; Lei, W. Magnesium Ions Promote the Biological Behaviour of Rat Calvarial Osteoblasts by Activating the PI3K/Akt Signalling Pathway. *Biol. Trace Elem. Res.* **2017**, *179*, 284–293.
- (28) Zhang, X.; He, Y.; Huang, P.; Jiang, G.; Zhang, M.; Yu, F.; Zhang, W.; Fu, G.; Wang, Y.; Li, W. A novel mineralized high strength hydrogel for enhancing cell adhesion and promoting skull bone regeneration in situ. *Composites, Part B* **2020**, *197*, No. 108183.
- (29) Yang, K.; Chen, Z.; Gao, J.; Shi, W.; Li, L.; Jiang, S.; Hu, H.; Liu, Z.; Xu, D.; Wu, L. The Key Roles of GSK-3 $\beta$  in Regulating Mitochondrial Activity. *Cell. Physiol. Biochem.* **2017**, *44*, 1445–1459.
- (30) Hur, E. M.; Zhou, F. Q. GSK3 Signalling in Neural Development. *Nat. Rev. Neurosci.* **2010**, *11*, 539–551.
- (31) Zhao, S.-J.; Kong, F.-Q.; Jie, J.; Li, Q.; Liu, H.; Xu, A.-D.; Yang, Y.-Q.; Jiang, B.; Wang, D.-D.; Zhou, Z.-Q.; Tang, P.-Y.; Chen, J.; Wang, Q.; Zhou, Z.; Chen, Q.; Yin, G.-Y.; Zhang, H.-W.; Fan, J. Macrophage MSR1 promotes BMSC osteogenic differentiation and M2-like polarization by activating PI3K/AKT/GSK3 $\beta$ / $\beta$ -catenin pathway. *Theranostics* **2020**, *10*, 17–35.
- (32) Zhang, T.; Chen, H.; Zhang, Y.; Zan, Y.; Ni, T.; Liu, M.; Pei, R. Photo-crosslinkable, bone marrow-derived mesenchymal stem cells-encapsulating hydrogel based on collagen for osteogenic differentiation. *Colloids Surf., B* **2019**, *174*, 528–535.
- (33) Huang, L.; Zhu, Z.; Wu, D.; Gan, W.; Zhu, S.; Li, W.; Tian, J.; Li, L.; Zhou, C.; Lu, L. Antibacterial poly (ethylene glycol) diacrylate/chitosan hydrogels enhance mechanical adhesiveness and promote skin regeneration. *Carbohydr. Polym.* **2019**, *225*, No. 115110.
- (34) Fu, S.; Ni, P.; Wang, B.; Chu, B.; Zheng, L.; Luo, F.; Luo, J.; Qian, Z. Injectable and thermo-sensitive PEG-PCL-PEG copolymer/

collagen/n-HA hydrogel composite for guided bone regeneration.

*Biomaterials* **2012**, *33*, 4801–4809.

(35) Vissers, C. A. B.; Harvestine, J. N.; Leach, J. K. Pore size regulates mesenchymal stem cell response to Bioglass-loaded composite scaffolds. *J. Mater. Chem. B* **2015**, *3*, 8650–8658.

(36) Taromsari, S. M.; Salari, M.; Bagheri, R.; Faghihi Sani, M. A. Optimizing tribological, tensile & in-vitro biofunctional properties of UHMWPE based nanocomposites with simultaneous incorporation of graphene nanoplatelets (GNP) & hydroxyapatite (HAp) via a facile approach for biomedical applications. *Composites, Part B* **2019**, *175*, No. 107181.

(37) Bee, S.-L.; Hamid, Z. A. A. Characterization of chicken bone waste-derived hydroxyapatite and its functionality on chitosan membrane for guided bone regeneration. *Composites, Part B* **2019**, *163*, 562–573.

(38) Kang, H.; Yang, B.; Zhang, K.; Pan, Q.; Yuan, W.; Li, G.; Bian, L. Immunoregulation of macrophages by dynamic ligand presentation via ligand–cation coordination. *Nat. Commun.* **2019**, *10*, No. 1696.

(39) Brown, D.; Gatter, K. J. H. Ki67 protein: the immaculate deception? *Histopathology* **2002**, *40*, 2–11.

(40) Wu, Y.-P.; Yang, J.; Gao, H.-Y.; Shen, Y.; Jiang, L.; Zhou, C.; Li, Y.-F.; He, R.-R.; Liu, M. Folate-conjugated halloysite nanotubes, an efficient drug carrier, deliver doxorubicin for targeted therapy of breast cancer. *ACS Appl. Nano Mater.* **2018**, *1*, 595–608.

(41) Vergadi, E.; Ieronymaki, E.; Lyroni, K.; Vaporidi, K.; Tsatsanis, C. Akt Signaling Pathway in Macrophage Activation and M1/M2 Polarization. *J. Immunol.* **2017**, *198*, 1006–1014.

(42) Lou, S.-j.; Gu, P.; Chen, F.; He, C.; Wang, M.-w.; Lu, C. L. The effect of bone marrow stromal cells on neuronal differentiation of mesencephalic neural stem cells in Sprague–Dawley rats. *Brain Res.* **2003**, *968*, 114–121.

(43) Lin, Z.; Wu, J.; Qiao, W.; Zhao, Y.; Wong, K. H.; Chu, P. K.; Bian, L.; Wu, S.; Zheng, Y.; Cheung, K. M. C.; et al. Precisely controlled delivery of magnesium ions thru sponge-like monodisperse PLGA/nano-MgO-alginate core-shell microsphere device to enable in-situ bone regeneration. *Biomaterials* **2018**, *174*, 1–16.